OXFORD

Human Molecular Genetics, 2017, Vol. 26, No. 11 2091–2103

doi: 10.1093/hmg/ddx104
Advance Access Publication Date: 15 March 2017
Original Article

ORIGINAL ARTICLE

Scn2a deletion improves survival and brain–heart dynamics in the *Kcna1*-null mouse model of sudden unexpected death in epilepsy (SUDEP)

Vikas Mishra[1], Bharat K. Karumuri[2], Nicole M. Gautier[1], Rui Liu[3], Timothy N. Hutson[2], Stephanie L. Vanhoof-Villalba[1], Ioannis Vlachos[3], Leonidas Iasemidis[2] and Edward Glasscock[1,*]

[1]Department of Cellular Biology and Anatomy, Louisiana State University Health Sciences Center, Shreveport, LA 71130, USA, [2]Biomedical Engineering, Louisiana Tech University, Ruston, LA 71272, USA and [3]Department of Mathematics and Statistics, Louisiana Tech University, Ruston, LA 71272, USA

*To whom correspondence should be addressed at: Department of Cellular Biology and Anatomy, Louisiana State University Health Sciences Center, 1501 Kings Highway, PO Box 33932, Shreveport, LA 71130-3932, USA. Tel: +318 6758886; Fax: +318 6755889; Email: aglas1@lsuhsc.edu

Abstract

People with epilepsy have greatly increased probability of premature mortality due to sudden unexpected death in epilepsy (SUDEP). Identifying which patients are most at risk of SUDEP is hindered by a complex genetic etiology, incomplete understanding of the underlying pathophysiology and lack of prognostic biomarkers. Here we evaluated heterozygous *Scn2a* gene deletion (*Scn2a*$^{+/-}$) as a protective genetic modifier in the *Kcna1* knockout mouse (*Kcna1*$^{-/-}$) model of SUDEP, while searching for biomarkers of SUDEP risk embedded in electroencephalography (EEG) and electrocardiography (ECG) recordings. The human epilepsy gene *Kcna1* encodes voltage-gated Kv1.1 potassium channels that act to dampen neuronal excitability whereas *Scn2a* encodes voltage-gated Nav1.2 sodium channels important for action potential initiation and conduction. SUDEP-prone *Kcna1*$^{-/-}$ mice with partial genetic ablation of Nav1.2 channels (i.e. *Scn2a*$^{+/-}$; *Kcna1*$^{-/-}$) exhibited a two-fold increase in survival. Classical analysis of EEG and ECG recordings separately showed significantly decreased seizure durations in *Scn2a*$^{+/-}$; *Kcna1*$^{-/-}$ mice compared with *Kcna1*$^{-/-}$ mice, without substantial modification of cardiac abnormalities. Novel analysis of the EEG and ECG together revealed a significant reduction in EEG–ECG association in *Kcna1*$^{-/-}$ mice compared with wild types, which was partially restored in *Scn2a*$^{+/-}$; *Kcna1*$^{-/-}$ mice. The degree of EEG–ECG association was also proportional to the survival rate of mice across genotypes. These results show that *Scn2a* gene deletion acts as protective genetic modifier of SUDEP and suggest measures of brain–heart association as potential indices of SUDEP susceptibility.

Introduction

Sudden unexpected death in epilepsy (SUDEP) is the leading cause of epilepsy-related mortality, but how to accurately predict which patients are most at risk remains obscured by a complex genetic basis and a lack of reliable biomarkers (1,2). A death is classified as SUDEP when an individual with epilepsy, who is otherwise healthy, dies with no pathological explanation even upon postmortem examination (3). Although the exact pathophysiological causes of SUDEP remain poorly understood, the primary suspected mechanism is that seizures somehow evoke cardiorespiratory arrest leading to death (4). SUDEP claims the lives of about 1/1000 patients with epilepsy every year, which translates to an estimated 2750 deaths annually in the United

Received: January 10, 2017. **Revised:** February 28, 2017. **Accepted:** March 13, 2017

States and an 8% cumulative risk of dying suddenly in patients with early onset epilepsy (5).

Although several genes, predominantly coding for different ion channels, have been linked to epilepsy in rare Mendelian pedigrees, most epilepsy is believed to involve multiple co-inherited or *de novo* genetic variants that combine to cause disease (6). However, identifying which gene variant combinations are beneficial or deleterious is complicated by the large number of non-synonymous variants, even of identified epilepsy genes, in both epilepsy patients and non-epilepsy control groups (7). Recent studies reveal that SUDEP is at least as genetically complex as epilepsy itself, involving polygenic interactions between genes related to epilepsy, cardiac arrhythmias, and respiratory dysfunction (8,9). Furthermore, exome-based analyses of DNA from SUDEP patients reveal that the genome-wide polygenic burden of rare deleterious variants in SUDEP hinders any single gene from rising to genome-wide significance (8,9).

The *Kcna1* gene encodes axonal voltage-gated Kv1.1 potassium channel α-subunits that dampen neuronal excitability by regulating action potential firing properties (10–12). Mice lacking Kv1.1 channels due to deletion of the *Kcna1* gene (*Kcna1*$^{-/-}$) are frequently used to study candidate genetic and pathophysiological mechanisms underlying SUDEP since they model multiple human SUDEP risk factors and terminal neurocardiac patterns. These similarities include (i) frequent seizures; (ii) generalized tonic–clonic seizures; (iii) early onset epilepsy; (iv) long duration of epilepsy; (v) young age; and (vi) seizure-evoked bradycardia and asystole progressing to cardiac arrest (13–17). Another prominent feature and proposed mechanism of human SUDEP is seizure-associated respiratory arrest (4), but extensive respiratory studies in *Kcna1*$^{-/-}$ mice have not been performed.

Patients heterozygous for *KCNA1* mutations exhibit neuronal hyperexcitability phenotypes, including epilepsy, episodic ataxia type 1 (EA1), and myokymia (18–20). Although the majority of human *KCNA1* variants are associated with EA1, at least four different loss-of-function missense mutations in *KCNA1* have been identified that cause epilepsy either with (T226R, V408L and F414S) or without (A242P) ataxia (19,21–23). These mutations all affect conserved regions of the transmembrane domains of the Kv1.1 subunit, including the S2 and S6 segments, and functionally they cause reduced surface expression of the channel, reduced current densities, and positive voltage shifts in activation (24). Mutation of the highly conserved S6 transmembrane pore domain segment can have especially severe functional effects rendering the Kv1.1 subunit nonfunctional, as observed for the epilepsy-causing F414S mutation (21). Furthermore, a *de novo* copy number variant in *KCNA1* affecting the protein-coding sequence of the S6 region was identified as a principal risk factor for the premature death of one SUDEP victim (25). However, unlike the *Kcna1*$^{-/-}$ mouse model, sudden death associated with *KCNA1* mutations has not been reported as a common feature of disease in patients, but this could be due partly to ascertainment bias. Since *KCNA1* is not a known long QT cardiac arrhythmia gene, it is not usually included in genetic screens related to human sudden death (26).

Previous studies have identified protective genetic modifiers that ameliorate epilepsy and prevent SUDEP in *Kcna1*$^{-/-}$ mice (27,28). When hypomorphic mutations in the synaptic P/Q-type Ca^{2+} channel gene (*Cacna1a)* or the tau axonal microtubule-binding protein gene *(Mapt)* are bred into *Kcna1*$^{-/-}$ mice, the resulting double mutants exhibited reduced seizure frequencies and greatly improved survival rates (27,28). To further dissect the complex genetic interactions and pathomechanisms underlying SUDEP, we examined the effects of partial genetic ablation of Nav1.2 channels on epilepsy and premature death in the *Kcna1*$^{-/-}$ mouse model. Voltage-gated Nav1.2 sodium channel α-subunits are encoded by the *Scn2a* gene and localize to axons and axon initial segments where they are important for action potential initiation and conduction (29,30). Heterozygous *Scn2a* knockouts (*Scn2a*$^{+/-}$) show no obvious deficits despite ∼50% reductions in Nav1.2 mRNA levels and sodium currents in hippocampal neurons (31). Given the mutually opposing effects on axonal excitability exerted by the *Scn2a* and *Kcna1* knockout mutations, we hypothesized that partial genetic removal of Nav1.2 channels due to heterozygous *Scn2a* gene deletion (*Scn2a*$^{+/-}$) would act as a protective genetic modifier of SUDEP, suppressing neurocardiac dysfunction and reducing lethality in *Kcna1*$^{-/-}$ mice. Finally, we employed a novel methodology to analyze concurrent EEG and ECG recordings from *Kcna1*$^{-/-}$ mice, double mutants (*Scn2a*$^{+/-}$; *Kcna1*$^{-/-}$), and controls, which involves quantifying the degree of association of the features extracted from the analysis of these brain and heart biosignals in search of biomarkers for SUDEP susceptibility at the systems level.

Results

Decreasing Nav1.2 levels prevents premature death in *Kcna1*$^{-/-}$ mice

To test whether decreasing neuronal excitability by *Scn2a* partial loss-of-function (*Scn2a*$^{+/-}$) would counterbalance the increased excitability caused by *Kcna1* loss-of-function (*Kcna1*$^{-/-}$) and lead to a decrease in SUDEP incidence, we generated double mutants with various combinations of *Scn2a* and *Kcna1* knockout alleles and monitored survival. In agreement with previous studies, *Kcna1*$^{-/-}$ mice (n = 44) began dying on P16 and only 40% of animals lived to 10 weeks (Fig. 1A). In contrast, *Scn2a*$^{+/-}$; *Kcna1*$^{-/-}$ mice (n = 116), which have Nav1.2 decreased by half, exhibited a significant two-fold increase in survival (Log-rank test, $P < 0.0001$) with 79% living to 10 weeks (Fig. 1A). Premature death was never observed in heterozygous *Scn2a*$^{+/-}$ mice (n = 33) without Kv1.1 deficiency (i.e. *Scn2a*$^{+/-}$; *Kcna1*$^{+/+}$), suggesting that a half dosage of Nav1.2 is sufficient for normal lifespan (Fig. 1A). Mice with a homozygous *Scn2a* knockout genotype (*Scn2a*$^{-/-}$) were never obtained in double mutant crosses since *Scn2a*$^{-/-}$ causes perinatal lethality (31). These data reveal a strong protective genetic modifier effect of heterozygous *Scn2a* gene deletion on SUDEP in *Kcna1*$^{-/-}$ mice.

Original characterization of the *Scn2a* knockout mutation demonstrated ∼50% reductions in *Scn2a* mRNA levels in heterozygous mice (*Scn2a*$^{+/-}$); however, protein levels were not quantified to verify a corresponding reduction in Nav1.2 subunits (31). Therefore, western blotting was performed to measure Nav1.2 protein levels in the cortex, hippocampus and brainstem of *Scn2a*$^{+/-}$ mice. Immunoblotting revealed a significant ∼50% reduction in Nav1.2 levels in cortex (two-tailed Student's *t* test, $P = 0.0002$), hippocampus ($P = 0.0104$), and brainstem ($P = 0.0031$) homogenates from *Scn2a*$^{+/-}$ mice compared with wild type (WT) controls (Fig. 1B and Supplementary Material, Fig. S1). These results confirm that heterozygous *Scn2a* deletion reduces Nav1.2 subunits by ∼50% at both the mRNA and protein levels.

Heterozygous *Scn2a* deletion ameliorates spontaneous seizure severity in *Kcna1*$^{-/-}$ mice

To determine the effects of heterozygous *Scn2a* deletion on spontaneous seizures and cardiac function in *Kcna1*$^{-/-}$ mice, *in vivo* video-EEG–ECG recordings were performed in single and

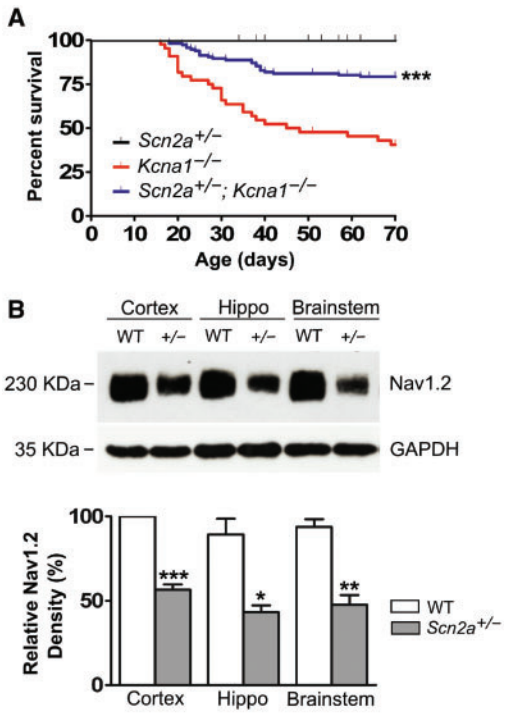

Figure 1. Nav1.2 reduction improves survival in *Kcna1*$^{-/-}$ mice. (**A**) Kaplan-Meier survival curves for *Scn2a*$^{+/-}$ mice (n = 33), *Kcna1*$^{-/-}$ mice (n = 44), and double mutant *Scn2a*$^{+/-}$; *Kcna1*$^{-/-}$ mice (n = 116). (**B**) Representative Western blots for Nav1.2 and GAPDH loading control from cortex, hippocampus (hippo), and brainstem of *Scn2a*$^{+/-}$ mice and WT animals with quantification of Nav1.2 protein levels in each brain region (n = 3/genotype). *$P < 0.05$; **$P < 0.01$; ***$P < 0.0001$.

double mutant mice. Single mutant *Kcna1*$^{-/-}$ mice (n = 9) exhibited frequent spontaneous seizures with electrographic characteristics similar to those previously reported for mice lacking Kv1.1 channels (13), including an initial large spike at seizure onset followed by brief voltage depression transitioning into high amplitude spiking and terminating in burst suppression patterns (Fig. 2A). Behaviorally, these episodes showed characteristics of limbic system seizures of varying severity, as previously reported in (16). Most seizures in *Kcna1*$^{-/-}$ mice were mild, characterized by head bobbing, forelimb/hindlimb clonus, tail extension, and often a single rearing event corresponding to stages 1–3 on the modified Racine scale described by Simeone *et al.* (16). However, at least four *Kcna1*$^{-/-}$ mice exhibited more severe seizures, which progressed to include continuous rearing and falling (stage 4) or tonic–clonic convulsions (stage 5). Double mutant mice (*Scn2a*$^{+/-}$; *Kcna1*$^{-/-}$; n = 8) displayed electrographic seizures that appeared qualitatively similar to seizures of comparable duration in single mutant *Kcna1*$^{-/-}$ mice (Fig. 2A). However, no stage 5 seizures were ever observed in double mutants suggesting a reduction in seizure severity. Singly heterozygous *Scn2a*$^{+/-}$ mice (n = 8) exhibited EEG recordings that were devoid of seizures and epileptiform discharges (Fig. 2A), similar to WT animals (n = 8).

Quantification of seizure incidence in *Kcna1*$^{-/-}$ and *Scn2a*$^{+/-}$; *Kcna1*$^{-/-}$ mice revealed similar seizure frequencies of 7.9 ± 3.1 and 6.4 ± 4.3 seizures per 24 h, respectively (two-tailed Student's *t* test, $P = 0.78$; Fig. 2B), suggesting that Nav1.2 ablation does not decrease seizure occurrence. However, seizure durations were significantly reduced by about 65% from 40 ± 9 s in *Kcna1*$^{-/-}$ mice to 14 ± 6 s in *Scn2a*$^{+/-}$; *Kcna1*$^{-/-}$ mice (two-tailed Student's *t* test, $P = 0.03$; Fig. 2C). Furthermore, about 35% of seizures (25/71) in *Kcna1*$^{-/-}$ mice lasted > 60 s, but only 2% of recorded seizures (1/51) exceeded 60 s in double mutants (Fig. 2D). The abbreviated seizure durations in *Scn2a*$^{+/-}$; *Kcna1*$^{-/-}$ mice led to a ~70% decrease in seizure burden (5 ± 2 s seizing/h) compared with *Kcna1*$^{-/-}$ animals (17 ± 7 s seizing/h; two-tailed Student's *t* test, $P = 0.13$; Fig. 2E). Interestingly, the highest seizure frequency was observed in one *Scn2a*$^{+/-}$; *Kcna1*$^{-/-}$ mouse (double mutant no. 3 in Fig. 2D), which exhibited 34 seizures in 24 h; however, all but 3 of those seizures were very brief in duration (≤15 s). To provide an additional assessment of seizure severity, a seizure burden score was calculated for each animal by taking into account both the duration of each seizure and the behavioral severity (see 'Materials and Methods' section). Seizure burden scores (SBSs) were 67% lower in *Scn2a*$^{+/-}$; *Kcna1*$^{-/-}$ mice relative to *Kcna1*$^{-/-}$ mice, indicative of reduced seizure severity in double mutants (Supplementary Material, Fig. S2). Overall, these results suggest that heterozygous *Scn2a* deletion decreases the incidence of premature death in *Kcna1*$^{-/-}$ mice by ameliorating seizure severity without significantly affecting seizure frequency.

To examine seizure severity in more detail, we compared the spectral power density of pre- and post-ictal periods for a representative subset of seizures of short (<31 s), intermediate (31–60 s), and long (>60 s) durations. In temporal lobe epilepsy patients, post-ictal spectral power shifts to progressively lower frequencies as seizure severity increases, providing an EEG marker of seizure severity (32). Spectral analysis revealed very similar distributions across EEG frequency bands before and after seizures of short and intermediate durations in *Kcna1*$^{-/-}$ and *Scn2a*$^{+/-}$; *Kcna1*$^{-/-}$ mice (Fig. 3A and B). However, following long seizures in *Kcna1*$^{-/-}$ mice, the post-ictal spectral power of the delta frequency band was significantly increased by ~50% compared with the pre-ictal baseline (two-tailed Student's *t* test, $P = 0.036$; Fig. 3A). In addition, the post-ictal power of the alpha ($P = 0.017$) and beta bands ($P = 0.0077$) exhibited a corresponding decrease compared with the pre-ictal period (two-tailed Student's *t* test; Fig. 3A). These post-ictal changes in the EEG power spectrum following long seizures in *Kcna1*$^{-/-}$ mice are indicative of post-ictal EEG slowing, which is a characteristic of severe seizures (32). Spectral power density could not be examined for long seizures in *Scn2a*$^{+/-}$; *Kcna1*$^{-/-}$ mice since they do not typically exhibit seizures lasting > 60 s. Thus, the long duration seizures in *Kcna1*$^{-/-}$ mice cause transient post-ictal disruptions in cortical activity that are not observed in the shorter duration seizures of double mutants.

Nav1.2 reduction does not increase seizure threshold in *Kcna1*$^{-/-}$ mice

To test whether heterozygous *Scn2a* deletion influences seizure threshold in *Kcna1*$^{-/-}$ mice, susceptibility to flurothyl-induced seizures was examined. Flurothyl (2,2,2-trifluoroethyl ether) is a volatile convulsant agent used for quantifying seizure susceptibility in mice since it reliably evokes generalized tonic–clonic behavioral seizures in rodents of all ages (33). Upon exposure to flurothyl, the mean latency to generalized tonic–clonic seizure in *Kcna1*$^{-/-}$ mice (199 ± 31 s; n = 3) was significantly reduced (one-way analysis of variance (ANOVA), Tukey's *post hoc*, $P < 0.0001$) compared with WT controls (494 ± 32 s; n = 5; Fig. 4A), indicating a decrease in seizure threshold as previously reported in (13,34). However, the seizure latencies of *Scn2a*$^{+/-}$; *Kcna1*$^{-/-}$ mice (238 ± 38 s; n = 5) were similar to *Kcna1*$^{-/-}$ animals, suggesting no alteration of seizure threshold

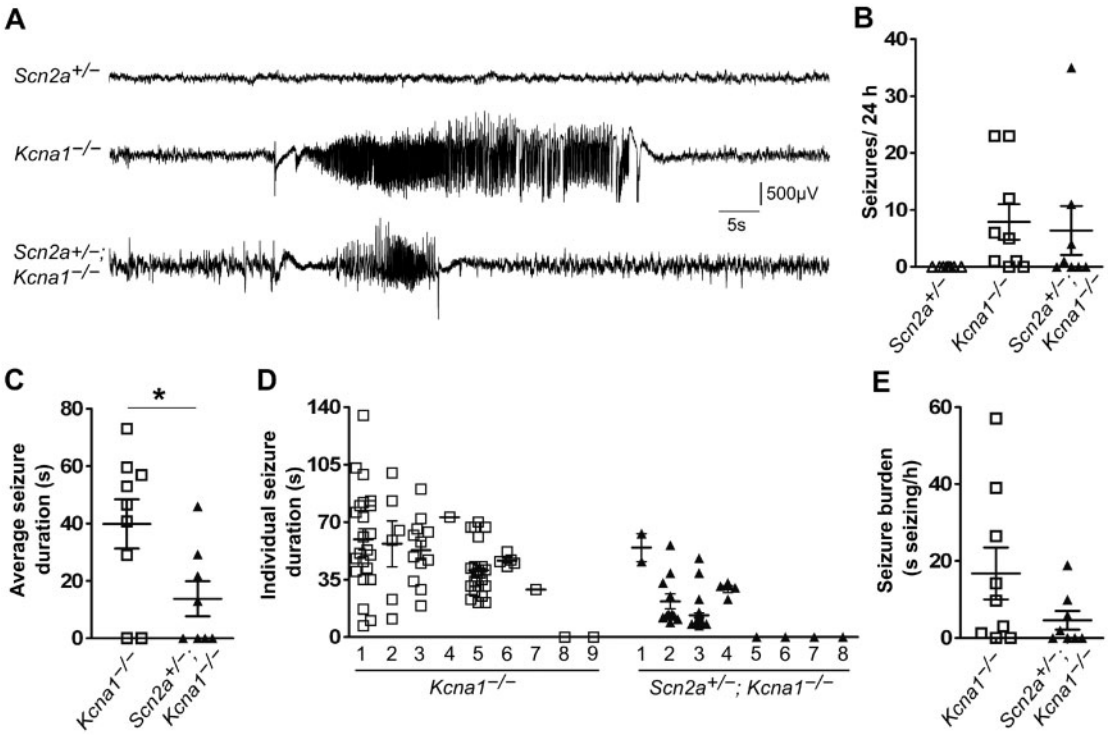

Figure 2. Nav1.2 reduction decreases seizure durations in *Kcna1*$^{-/-}$ mice. (**A**) EEG traces showing representative seizure activity in *Kcna1*$^{-/-}$ and *Scn2a*$^{+/-}$; *Kcna1*$^{-/-}$ mice and the absence of epileptiform activity in *Scn2a*$^{+/-}$ animals. (**B**) Quantification of seizure frequency in *Scn2a*$^{+/-}$ mice (n = 8), *Kcna1*$^{-/-}$ mice (n = 9) and *Scn2a*$^{+/-}$; *Kcna1*$^{-/-}$ mice (n = 8; $P = 0.78$). Seizures were never observed in *Scn2a*$^{+/-}$ mice. In addition, seizures were not observed in two *Kcna1*$^{-/-}$ animals. This absence was likely due to the sampling period being limited to 24 h and not indicative of the absence of epilepsy in these animals. (**C**) Quantification of average seizure duration in *Kcna1*$^{-/-}$ mice and *Scn2a*$^{+/-}$; *Kcna1*$^{-/-}$ mice ($P = 0.03$). (**D**) Plot of individual seizure durations for every seizure recorded in each *Kcna1*$^{-/-}$ and *Scn2a*$^{+/-}$; *Kcna1*$^{-/-}$ animal in the study. (**E**) Quantification of seizure burden (time spent seizing per h) in *Kcna1*$^{-/-}$ and *Scn2a*$^{+/-}$; *Kcna1*$^{-/-}$ mice ($P = 0.13$). *$P < 0.05$.

by the *Scn2a* null allele (Fig. 4A). Furthermore, heterozygous *Scn2a*$^{+/-}$ mice exhibited seizure latencies that were indistinguishable from WT mice (Fig. 4A), which is an additional indication that a half dosage of Nav1.2 channels does not by itself significantly alter seizure threshold. Comparison of the mean latencies to the first myoclonic jerk revealed a similar relationship between genotypes as that observed for the mean seizure latencies: WT and *Scn2a*$^{+/-}$ mice exhibited the longest latencies, while *Kcna1*$^{-/-}$ and *Scn2a*$^{+/-}$; *Kcna1*$^{-/-}$ mice exhibited similarly shortened latencies (Fig. 4B). These results suggest that the protective effects of *Scn2a* deletion do not act at the level of seizure threshold.

Heterozygous *Scn2a* deletion does not modify cardiac dysfunction in *Kcna1*$^{-/-}$ mice

To determine whether *Scn2a* deletion exerts a protective effect on heart function in *Kcna1*$^{-/-}$ mice, cardiac activity was analyzed using the *in vivo* video-EEG–ECG recordings. As observed in our previous study (15), *Kcna1*$^{-/-}$ mice exhibited an increased frequency of interictal skipped heart beats (1.9 ± 0.6/h), a roughly three- to four-fold increase compared with *Scn2a*$^{+/-}$ (0.7 ± 0.2/h) and WT mice (0.5 ± 0.2/h), respectively (one-way ANOVA, $P = 0.056$; Fig. 5A and B). Skipped heart beats in *Kcna1*$^{-/-}$ mice occur due to atrioventricular (AV) conduction blocks that are vagally driven since they are abolished by the parasympathetic blocker atropine (15). Although these conduction blocks are likely benign, they provide a biomarker of abnormal cardiac function indicative of potential autonomic dysregulation. Double mutant *Scn2a*$^{+/-}$; *Kcna1*$^{-/-}$ mice showed similar numbers of skipped heart beats (1.5 ± 0.3/h) to *Kcna1*$^{-/-}$ mice (Fig. 5A and B), suggesting no significant amelioration of cardiac dysfunction at the level of AV electrical conduction.

Kcna1$^{-/-}$ mice also exhibit ictal bradycardia and improved survival following vagotomy, suggesting underlying parasympathetic dysfunction that may contribute to their premature death (14,15). To assess the influence of the parasympathetic branch of the autonomic nervous system on cardiac function, heart rate variability (HRV) was calculated in the time domain for each genotype using the following measures: the standard deviation of the beat-to-beat intervals (SDNN), which is an index of total autonomic variability; and the root mean square of successive beat-to-beat differences (RMSSD), which is an index of parasympathetic tone (35). Mean heart rates were similar between all genotypes (one-way ANOVA, $P = 0.39$; Fig. 5C). SDNN was elevated in *Kcna1*$^{-/-}$ and *Scn2a*$^{+/-}$; *Kcna1*$^{-/-}$ mice compared with *Scn2a*$^{+/-}$ and WT controls, but these differences were not statistically significant between genotypes (one-way ANOVA, $P = 0.069$; Fig. 5D). However, RMSSD exhibited a significant ≥ 2-fold increase in *Kcna1*$^{-/-}$ mice compared with *Scn2a*$^{+/-}$ and WT mice (one-way ANOVA, Tukey's *post hoc*, $P = 0.0092$; Fig. 5E), providing further evidence of abnormally high parasympathetic tone in mice lacking Kv1.1 channels. Double mutant *Scn2a*$^{+/-}$; *Kcna1*$^{-/-}$ mice also exhibited increased RMSSD values similar to *Kcna1*$^{-/-}$ mice (Fig. 5E), but they were not significantly different from WT and *Scn2a*$^{+/-}$ mice (Tukey's *post hoc*, $P = 0.084$ and 0.14, respectively). These findings suggest that Nav1.2 reduction does not exert protective effects by modifying basal parasympathetic control of the heart.

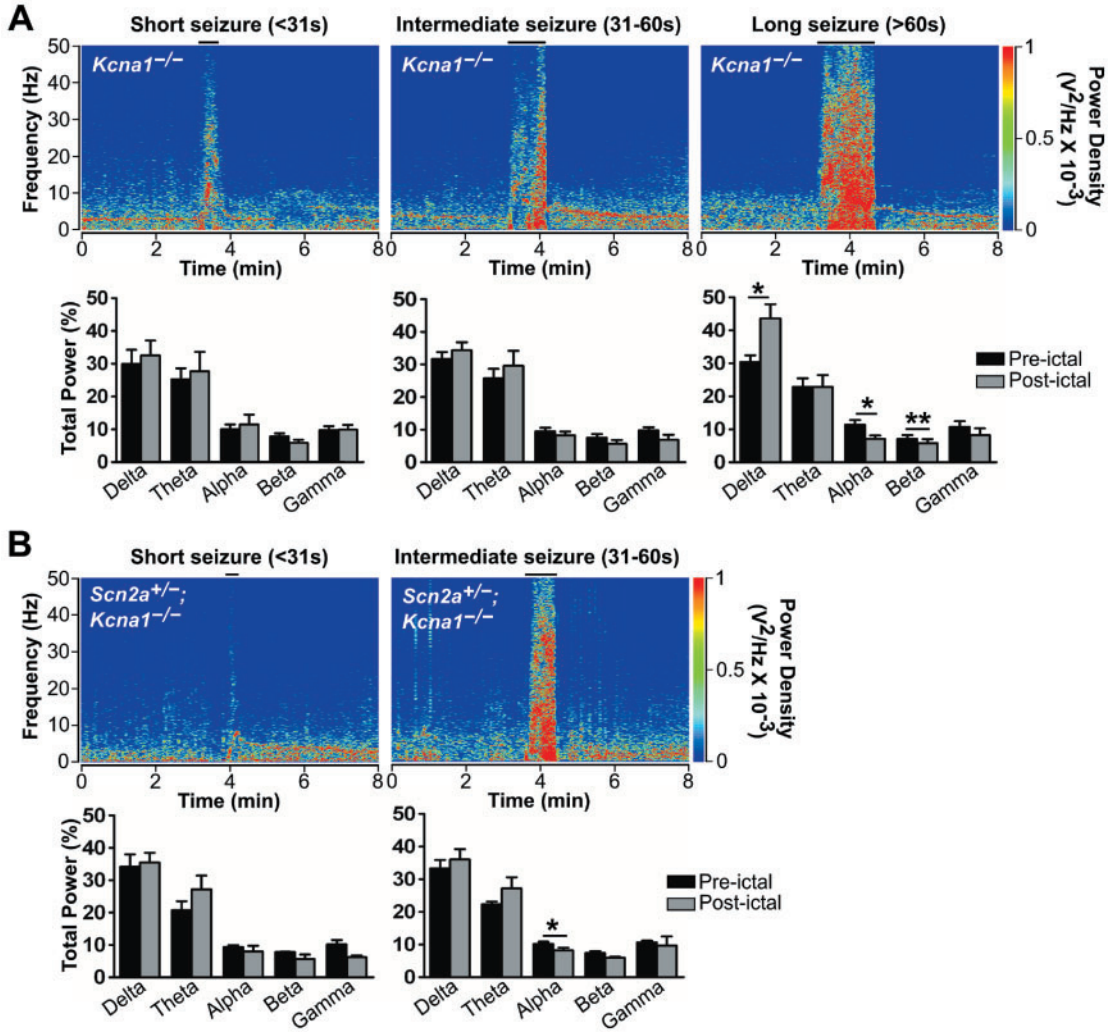

Figure 3. Long duration seizures in *Kcna1*$^{-/-}$ mice cause post-ictal EEG slowing. Representative peri-ictal spectrograms showing frequency and power density before, during, and after spontaneous seizures of short (<31 s; n = 5), intermediate (31–60 s; n = 5), and long duration (>60 s; n = 5) in *Kcna1*$^{-/-}$ mice (**A**) and *Scn2a*$^{+/-}$; *Kcna1*$^{-/-}$ mice (**B**). Seizures are indicated by black bars above the spectrograms. Corresponding bar charts show quantitative comparison of the relative power in each EEG frequency band during the pre- and post-ictal periods. *$P < 0.05$; **$P < 0.01$.

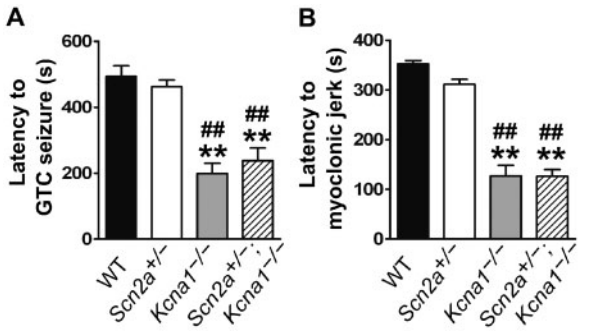

Figure 4. Nav1.2 reduction does not modify flurothyl-induced seizure threshold in *Kcna1*$^{-/-}$ mice. Quantification of the latency to generalized tonic–clonic (GTC) seizure (**A**) and the latency to first myoclonic jerk (**B**) upon exposure to flurothyl in WT (n = 5), *Scn2a*$^{+/-}$ (n = 5), *Kcna1*$^{-/-}$ (n = 3), and *Scn2a*$^{+/-}$; *Kcna1*$^{-/-}$ mice (n = 5). **$P < 0.001$ (one-way ANOVA, Tukey's *post hoc*; WT control). ##$P < 0.001$ (one-way ANOVA, Tukey's *post hoc*; *Scn2a*$^{+/-}$ mice).

Kcna1$^{-/-}$ mice exhibit decreased brain–heart association that is partially restored by *Scn2a* deletion

To further explore potential protective effects of heterozygous *Scn2a* deletion on brain–heart interactions in *Kcna1*$^{-/-}$ mice, we developed a new bioengineering-based analytical technique, which we term 'interaction dynamics', to measure the interaction between the brain and heart over time. In brief (see 'Materials and Methods' section for details), the simultaneously recorded EEG and ECG signals for each animal were divided into segments of 10 s in duration. The EEG signals were analyzed with respect to their complexity using Shannon's Entropy (ENT) for the traditional frequency bands (δ, θ, α, β and γ), and the ECG signals with respect to the complexity (ENT), median value (M) and interquartile range (IQR) of the RR intervals and R peaks. The EEG and ECG measures for each 10-s segment were then binarized, and their degree of association throughout the whole recording was evaluated using the phi (φ) coefficient. Higher φ coefficient values denote a higher degree of EEG–ECG (i.e. brain–heart) association.

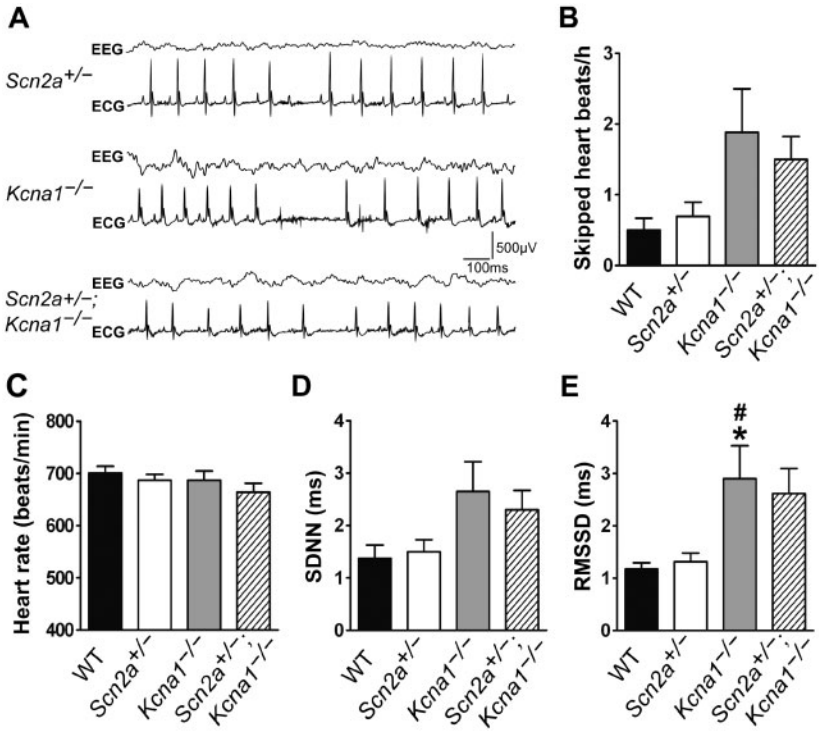

Figure 5. Nav1.2 reduction does not ameliorate cardiac phentoypes in *Kcna1*$^{-/-}$ mice. (**A**) Simultaneous EEG–ECG recordings showing representative skipped heart beats in *Scn2a*$^{+/-}$ mice, *Kcna1*$^{-/-}$ mice, and *Scn2a*$^{+/-}$; *Kcna1*$^{-/-}$ mice. (**B**) Quantification of the frequency of skipped heart beats (i.e. cardiac conduction blocks) across genotypes (n = 8/genotype; $P = 0.056$). (**C**) Quantification of mean heart rate across genotypes. (**D, E**) Quantification of HRV using the time domain measures of SDNN, an index of total autonomic variability (D); and the RMSSD, an index of parasympathetic tone (E). $^{*}P < 0.05$ (one-way ANOVA, Tukey's *post hoc*, WT mice). $^{\#}P < 0.05$ (one-way ANOVA, Tukey's *post hoc*, *Scn2a*$^{+/-}$ mice).

Qualitatively (Fig. 6A), WT mice generally exhibited a negative correlation between the duration of cardiac RR intervals (M_{RR}) and EEG signal complexity (ENT_α) implying that local maxima of heart rate may normally be associated with local maxima of EEG entropies in the α band. In *Kcna1*$^{-/-}$ mice, no association was apparent between the respective profiles from the heart and brain. Double mutant mice exhibited M_{RR} and ENT_α profiles with an intermediate degree of association. We used φ coefficients to quantify the relation between the estimated EEG and ECG feature profiles. WT mice exhibited the highest levels of association between brain and heart, while *Kcna1*$^{-/-}$ mice exhibited the lowest (Fig. 6B). The brain–heart association values in *Scn2a*$^{+/-}$ and *Scn2a*$^{+/-}$; *Kcna1*$^{-/-}$ mice were intermediate between those two extremes. ANOVA analysis based on the estimated φ coefficients between M_{RR} and ENT_α profiles showed statistically significant differences between genotypes (Welch's ANOVA with false discovery rate (FDR) adjusted $P = 0.029$). *Post hoc* analysis with Tukey's HSD test showed a statistically significant difference between *Kcna1*$^{-/-}$ and WT mice ($P < 0.003$), as well as between *Kcna1*$^{-/-}$ and *Scn2a*$^{+/-}$ genotypes ($P = 0.015$). These results together suggest that *Kcna1*$^{-/-}$ mice exhibit abnormal dissociation of brain and heart activity, which is partially restored in double mutants. The β band was the only other EEG band that showed statistically significant (FDR adjusted $P = 0.029$) and comparable results to the ones from the α band (see Supplementary Material, Table S1 and Supplementary Material, Fig. S3A and B). In Supplementary Material, Table S1, the FDR adjusted *P* values from the ANOVA procedure using the φ coefficients between all estimated EEG and ECG measures of dynamics (features) are shown. Indeed, significant differences between genotypes were identified only for the (M_{RR}, ENT_α) and (M_{RR}, ENT_β) pairs of features.

Finally, we investigated if any relationship existed across genotypes between the estimated brain–heart association values (φ coefficients) and survival rate. Using a linear fit (MATLAB subroutine 'fitlm') of the estimated φ coefficients between M_{RR} and ENT_α profiles from each recorded mouse and the 70-day survival rate per genotype (Fig. 1A), a statistically significant (linear regression, FDR adjusted $P = 0.0035$) positive linear trend between brain–heart association and survival rate was identified ($R^2 = 0.376$; Fig. 6C). These findings indicate that survival rate is proportional to brain–heart association, and that measures of brain–heart association could be useful in assessing the risk of susceptibility to SUDEP. Similar to the identification of statistically significant differences across genotypes, the β band was the only other EEG band (see Supplementary Material, Table S2 and Supplementary Material, Fig. S3C) that showed a statistically significant linear trend and comparable results to the ones from the α band ($R^2 = 0.375$; FDR adjusted $P = 0.0035$).

To determine whether the longer seizure durations and post-ictal EEG slowing in *Kcna1*$^{-/-}$ mice are responsible for their EEG–ECG dissociation, we performed additional analyses of the recordings that (i) excluded seizures (i.e. examination of interictal periods only); (ii) excluded seizures and the 5-min postictal period for each seizure; and (iii) excluded seizures and the 10-min postictal period for each seizure. The φ coefficients for the (M_{RR}, ENT_α) and (M_{RR}, ENT_β) pairs of features and the positive linear trend between the φ coefficients and survival rate did not change significantly by excluding these ictal and post-ictal timepoints (Supplementary Material, Fig. S4 and Supplementary Material, Table S3). Thus, the presence or absence of seizures on EEG does not significantly influence the degree of brain–heart association in our mice.

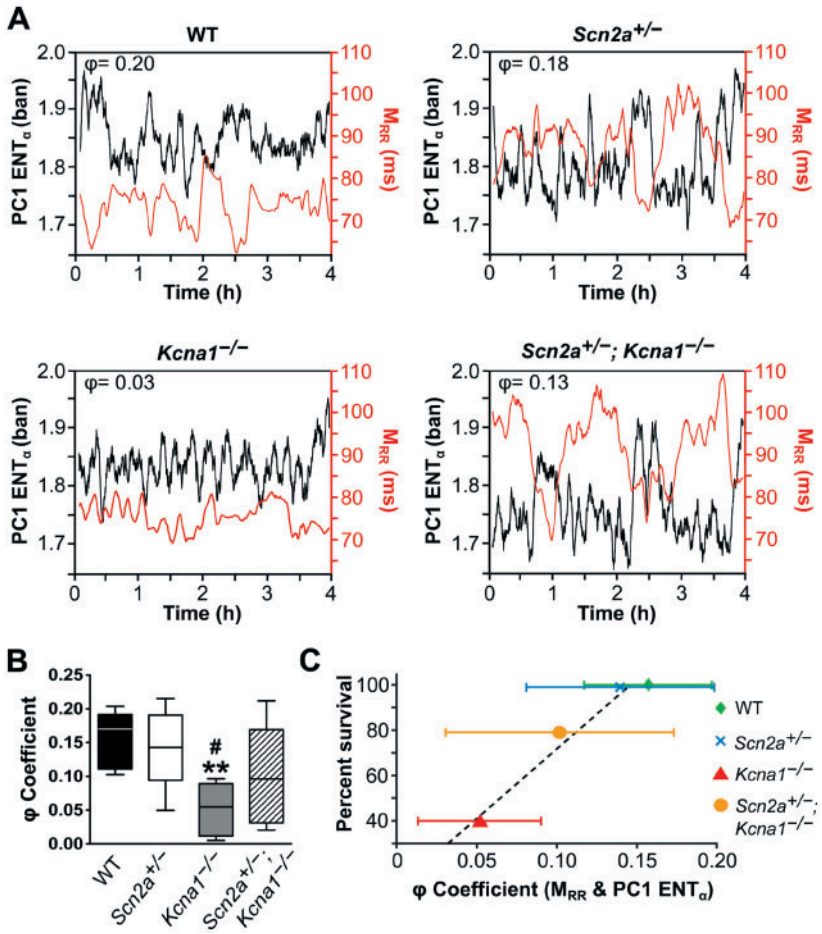

Figure 6. *Kcna1*$^{-/-}$ mice exhibit decreased brain–heart association that is partially restored by Nav1.2 reduction. (**A**) Representative profiles of the entropy of the first principal component of the EEG in the α band (PC1 ENT$_\alpha$) and the median of the RR intervals of the ECG (M_{RR}) over a 4-h epoch. The measures were estimated from sequential non-overlapping 10-s EEG and ECG segments and subsequently smoothed over 5 min for illustration purposes only, for one mouse from each genotype. The estimated ϕ coefficients between the PC1 ENT$_\alpha$ and M_{RR} profiles are specified on each plot. The entropy units are given in bans (log base 10 estimation of the entropy). (**B**) Quantification of brain–heart association by ϕ coefficients for each genotype (n = 8/genotype). The box plots show median values (solid horizontal line), IQR (box outline), and 1.5 × IQR (whiskers). (**C**) Plot of the survival percentage of each genotype versus the ϕ coefficients. Although the linear fit was performed on the individual data points, the data are shown as the mean ± SD for each genotype (linear regression, FDR adjusted $P = 0.0035$). $^{**}P < 0.01$ (Welch's ANOVA, Tukey's *post hoc*; WT mice). $^{\#}P < 0.05$ (Welch's ANOVA, Tukey's *post hoc*; *Scn2a*$^{+/-}$ mice).

Discussion

The genetic landscape of epilepsy and SUDEP is complex with interactions between multiple genes combining to cause disease and susceptibility to sudden death. In this study, we demonstrated a beneficial epistatic role for *Scn2a* gene deletion in preventing premature death and reducing seizure durations in the *Kcna1*$^{-/-}$ mouse model of SUDEP. Partially ablating Nav1.2 channels by heterozygous *Scn2a* gene deletion led to a dramatic improvement in survival rates of *Kcna1*$^{-/-}$ mice, which lack Kv1.1 channels. Although seizure frequency and seizure threshold remained unaltered, genetic ablation of Nav1.2 significantly reduced the duration of spontaneous seizures in *Kcna1*$^{-/-}$ mice. The long-duration seizures in *Kcna1*$^{-/-}$ mice led to post-ictal EEG slowing, a marker of seizure severity, which was absent in the abbreviated seizures of *Scn2a*$^{+/-}$; *Kcna1*$^{-/-}$ double mutants. Traditional ECG analysis of skipped heart beats, heart rate, and HRV revealed no significant modification of cardiac phenotypes by Nav1.2 reduction. However, analysis of EEG–ECG interaction dynamics revealed significantly decreased brain–heart association in *Kcna1*$^{-/-}$ mice that was partially restored in *Scn2a*$^{+/-}$; *Kcna1*$^{-/-}$ double mutants. These findings enhance our understanding of gene modifier interactions in epilepsy and SUDEP, and identify brain–heart association as a potential new biomarker of SUDEP risk stratification in epilepsy.

Evaluating SUDEP risk based on patient genetic profiles is currently hindered by the sheer number and complex combinations of ion channel gene variants that occur in both epilepsy patients and healthy controls (7–9). One approach to begin dissecting phenotypic causation amid this genetic complexity is to identify potential genetic modifiers using a reverse genetic, hypothesis-driven approach in model organisms, such as performed in this study (36). Genetic modifiers provide valuable information on disease pathophysiology and the identity of the responsible underlying genes and pathways (36). Furthermore, beneficial modifiers that mask disease phenotypes, known as genetic suppressors, represent potential gene targets for therapeutic intervention (6).

Here we showed that heterozygous *Scn2a* gene deletion acts as a dominant suppressor of SUDEP in *Kcna1*$^{-/-}$ mice by increasing survival, decreasing seizure duration, and partially

normalizing brain–heart association. The ability of Nav1.2 reduction to counteract the effects of Kv1.1 deficiency is likely due to the complementary expression patterns of the two genes at the regional and subcellular levels in the brain and the mutually opposing excitability defects of the two channel mutations; however, we did not directly measure excitability at the cellular level in this study. Nav1.2 channels are primarily expressed in unmyelinated axons and axon initial segments in brain regions implicated in epilepsy such as the hippocampus and cortex (37). Similarly, Kv1.1 channels are also predominantly axonal, localizing to unmyelinated axons, juxtaparanodes of myelinated axons, and axon initial segments, with prominent expression in hippocampus (38). A 50% reduction in Nav1.2 subunits causes drastic decreases in sodium currents in hippocampal pyramidal neurons that leads to decreased excitability, whereas the absence of Kv1.1 channels increases the frequency of epileptiform network burst discharges in the hippocampus (27,31). The reduction in Nav1.2 expression in the brainstem of *Scn2a*$^{+/-}$ mice, where it is normally expressed at high levels (Fig. 1B), may also provide a critical brake on excitability to prevent deleterious seizure-evoked spreading depolarization that could lead to cardiorespiratory arrest (31,39). Future electrophysiological studies will be required to assess how the two gene mutations interact to modify excitability and to identify the exact neuronal compartments and networks underlying this interaction.

Previous studies have identified two other genetic modifiers capable of ameliorating *Kcna1*$^{-/-}$ pathology: the *tottering (tg)* mutation of the *Cacna1a* gene and a knockout mutation of the *Mapt* gene (27,28). The *Cacna1a* gene encodes the pore-forming α1A-subunit of P/Q-type Ca^{2+} channels that mediates neurotransmitter release at terminals (40,41). *Kcna1*$^{-/-}$ mice that are homozygous or heterozygous for the partial loss-of-function *Cacna1a*^{tottering} allele exhibit drastic increases in survival (27). In addition, *Cacna1a*$^{tg/tg}$; *Kcna1*$^{-/-}$ mice exhibit concomitant reductions in seizure frequency and duration; however, seizure frequency and duration are not significantly modified in *Cacna1a*$^{tg/+}$; *Kcna1*$^{-/-}$ mice (27). The *Mapt* gene encodes the microtubule-binding protein tau, which is important for axonal transport and aggregates to form pathological neurofibrillary tangles in neurodegenerative disorders such as Alzheimer's disease (42). Tau loss due to *Mapt* gene deletion also drastically increases survival in *Kcna1*$^{-/-}$ mice and significantly decreases seizure frequency and duration; however, the mechanisms by which tau regulates neuronal excitability are still poorly understood (28).

Comparing our findings with these previous studies, the ability of the *Scn2a*$^{+/-}$ mutation to prevent SUDEP in *Kcna1*$^{-/-}$ mice is similar to the *Cacna1a*$^{tg/+}$ mutation in *Kcna1*$^{-/-}$ mice (79 versus 74% survival, respectively), but greater than the *Mapt*$^{+/-}$ mutation in *Kcna1*$^{-/-}$ mice (79 versus 59% survival, respectively) (27,28). However, heterozygous *Scn2a* gene deletion is unique among these dominant genetic suppressors for its ability to significantly decrease seizure duration without drastically affecting seizure frequency, suggesting Nav1.2 reduction may abrogate seizure activity once it is triggered without modulating seizure initiation. The lack of changes in flurothyl-induced seizure threshold in *Scn2a*$^{+/-}$; *Kcna1*$^{-/-}$ double mutants further supports this notion. Taken together with these previous studies, our work identifies axons and terminals as potentially effective subcellular targets for therapeutic modulation of excitability for the prevention of SUDEP. Thus, this study expands the range of genetic suppressor pathways for *Kcna1* channelopathy to include not only calcium channels regulating neurotransmitter release but also sodium channels controlling action potential firing.

A potential therapeutic implication of this study is the targeting of Nav1.2 channels for the treatment of epilepsy and prevention of SUDEP. In patients, heterozygosity for loss-of-function mutations in *SCN2A* are responsible for a broad spectrum of clinical neurological phenotypes ranging from mild and severe epilepsies (e.g. benign familial neonatal-infantile seizures and early onset infantile epileptic encephalopathy, respectively) to autism spectrum disorders and intellectual disability (43–50). However, this study shows that reducing Nav1.2 channel expression by half is not epileptogenic in mice since *Scn2a*$^{+/-}$ animals did not exhibit spontaneous seizures or reduced seizure thresholds. Therefore, heterozygosity for *Scn2a* loss-of-function mutations may have different neurological consequences in mice and humans, or the human mutations may lead to complex changes in the biophysical properties of the channels rather than simple haploinsufficiency (44). Furthermore, Nav1.2 channels are barely detectable in the heart and *Scn2a*$^{+/-}$ mice did not show any obvious cardiac abnormalities, suggesting that drugs targeting Nav1.2 channels have the advantage of minimal potential for unwanted cardiac side effects (51).

Given the central role of voltage-gated sodium channels in initiating action potentials in neurons, it is perhaps not surprising that they are the primary target of about half of the anticonvulsant drugs currently approved for the treatment of epilepsy by the Food and Drug Administration in the United States (52). The classical and widely used sodium channel-blocking anticonvulsant drugs such as phenytoin, carbamazepine, and lamotrigine share a similar mechanism of action, binding to common receptor sites in the pore-forming S6 segments of the channels, which inhibits sodium permeation in a voltage- and frequency-dependent manner (53). In *megencephaly* mice, which carry a truncation mutation in *Kcna1*, carbamazepine reduces seizure duration and severity without eliminating seizures, similar to the effects of partial genetic ablation of Nav1.2 (54). Interestingly, in addition to sodium channel blockade, lamotrigine also inhibits P-type Ca^{2+} channels and enhances K^+ repolarizing currents, which could render it particularly effective in treating *Kcna1* channelopathy, but this remains to be tested in *Kcna1*$^{-/-}$ mice (55,56). Currently, specific targeting of Nav1.2 channels with these classical sodium channel blocking drugs is not possible since they are generally non-selective for the major sodium channel subtypes, Nav1.1-Nav1.7 (53). A drawback to this lack of subunit selectivity is that some sodium channel blockers may be contraindicated in epilepsy patients with mutations in specific sodium channel subtypes because they can exacerbate seizures (53,57,58). However, this potential proepileptic effect may not be a limitation for treatment of *Kcna1* channelopathy given the positive effects of carbamazepine treatment in *megencephaly* mice (54). Therefore, although targeted reduction or inhibition of Nav1.2 channels has the advantage of minimal impact on cardiac function, it may lead to risk for adverse neurological effects in patients, and it may not be effective in all epilepsy cases.

In this study, we developed and employed a new EEG–ECG analytical technique, which we termed interaction dynamics, to evaluate the association between brain and heart activity in mice. Mathematical analysis of physiological signals has found numerous applications in epilepsy research. Largely centered on the EEG signal, quantitative analysis can provide valuable diagnostic and predictive tools for seizure detection, prediction, and epileptogenic focus localization (59–61). Since epilepsy is considered primarily a neurological disorder, ECG signals are not usually of principal focus. However, in the case of SUDEP,

cardiac signals may be equally important, especially when both are studied in concurrence. The study of brain–heart association through advanced mathematical analysis of biomedical signals and images was the theme of the most recent special issue of the journal of Philosophical Transactions of the Royal Society A (62). The authors emphasized the significance of such a combined analysis as a novel and promising avenue towards our understanding of the pathophysiology of several neurological and cardiovascular diseases.

We herein reported results from analysis of concurrent EEG and ECG recordings and quantification of their interaction dynamics in well-organized cohorts of mice with different levels of SUDEP risk. As far as we know, this study is the first of its kind to analyze the interaction dynamics between EEG and ECG as a potential biomarker for risk stratification in epilepsy and SUDEP. Our results point to a significantly reduced association between EEG and ECG in SUDEP, as manifested by the entropy in the EEG α and β bands and the duration of the RR intervals, when compared with the observed association in healthy WT animals. Furthermore, examination of the relationship between survival rate and EEG–ECG association reveals that EEG–ECG association may span a continuum between SUDEP and healthy states. Therefore, measures of EEG–ECG association could potentially be used as a global index of well-being in patients with epilepsy, a proposition that needs to be addressed more extensively with relevant animal and clinical studies in the near future. Additional studies will also be needed to explore the interactions of the brain and heart with respiration since respiratory dysregulation is another important candidate mechanism of SUDEP (4).

In conclusion, these findings expand our knowledge on the possible ion channel profiles ('channotypes') and pathomechanisms that converge to modify disease severity and risk of sudden death in epilepsy. The new biosignal interaction dynamics analysis technique employed herein suggests measures of brain–heart association as potential new indices to stratify risk for sudden death in epilepsy. The power of concurrent analysis of EEG–ECG interaction dynamics lies in its ability to uncover signs of deleterious neurocardiac dysfunction that are not readily apparent by classical analysis of the EEG and ECG in isolation.

Materials and Methods

Animals and genotyping

Double mutant mice carrying various combinations of *Scn2a* and *Kcna1* null alleles were generated by crossing F1 double heterozygotes (*Scn2a*$^{+/-}$; *Kcna1*$^{+/-}$) in a mixed Black Swiss (Tac:N:NIHS-BC) x C57BL/6J genetic background. The F1 double heterozygotes were obtained by crossing heterozygous *Scn2a*-null (*Scn2a*$^{+/-}$; C57BL/6J background) mice and heterozygous *Kcna1*-null (*Kcna1*$^{+/-}$; Tac:N:NIHS-BC background) mice. The *Kcna1* knockout (KO) allele was generated by targeted deletion of the entire open reading frame of the *Kcna1* gene (chromosome 6), as previously described in (13). The *Scn2a* KO allele was created by targeted deletion of the first half of exon 1 of the *Scn2a* gene (chromosome 2), as previously described in (31). Mice were housed at ∼22 °C, fed *ad libitum*, and submitted to a 12-h light/dark cycle. All procedures were performed in accordance with the guidelines of the National Institutes of Health (NIH), as approved by the Institutional Animal Care and Use Committee of the Louisiana State University Health Sciences Center-Shreveport.

For genotyping, genomic DNA was isolated by enzymatic digestion of tail clips using Direct-PCR Lysis Reagent (Viagen Biotech, Los Angeles, CA, USA). Genotypes were determined by performing PCR amplification of genomic DNA using allele-specific primers, as previously described (31,63). For *Kcna1*, the following primer sequences were used to yield amplicons of ∼337 bp for the WT allele and ∼475 bp for the KO allele: a mutant specific primer (5′-CCTTCTATCGCCTTCTTGACG-3′), a WT specific primer (5′-GCCTCTGACAGTGACCTCAGC-3′), and a common primer (5′-GCTTCAGGTTCGCCACTCCCC-3′). For *Scn2a*, the following primer sequences were used to yield amplicons of ∼450 bp for the WT allele and ∼1300 bp for the KO allele: a forward sense primer (5′-TGCGAGGAGCTAAACAGTGATTAAAG-3′) and a reverse antisense primer (5′- GGCTCCATTCCCTTATCAG ACCTACCC-3′).

Western blotting

Age-matched *Scn2a*$^{+/-}$ and WT mice of both sexes (ages 2–3 months) were anesthetized with isoflurane and the brains quickly removed and dissected to separate cortex, hippocampus and brainstem. Tissues were homogenized with a mechanical shearer in ten volumes of ice-cold RIPA buffer (pH 7.4; Thermo Scientific, Waltham, MA) containing EDTA and a cocktail of protease inhibitors. Tissue homogenates were centrifuged at 9300 relative centrifugal force for 10 min at 4 °C to remove nuclei and cellular debris. The supernatants containing the crude membrane fractions were collected and stored at −80 °C until used. Protein concentrations of the brain homogenates were determined using Bradford reagent (Bio-Rad Laboratories, Hercules, CA) and equal amounts of protein were resolved on 7.5% SDS-polyacrylamide gels by electrophoresis. Proteins were then transferred onto nitrocellulose membranes by wet transfer at 4 °C. The non-specific binding sites on the membranes were blocked by incubating them for 1 h at room temperature (RT; ∼22 °C) in blocking buffer made of phosphate buffered saline-Tween (PBST; 0.1% v/v) and milk protein (5% w/v) and then incubated overnight at 4 °C with primary antibody solution prepared in blocking buffer. The primary antibodies used were mouse monoclonal antiNav1.2 (1:500; K69/3; NeuroMab, Davis, CA) and goat polyclonal antiGAPDH HRP (1:500; V-18; Santa Cruz Biotechnology, Dallas, TX). Following overnight incubation, the membranes treated with antiNav1.2 primary antibodies were washed three times for 5 min with PBST and incubated for 1 h at RT with goat antimouse IgG-HRP secondary antibody (1:1000; Santa Cruz Biotechnology, Dallas, TX) in blocking buffer. After a final wash in PBST, immunoreactive bands were visualized by an enhanced chemiluminiscence detection kit (GE Healthcare, Pittsburgh, PA) and developed on Amersham hyperfilm. Band intensity was quantified by spot densitometry analysis using ImageJ software (NIH; Bethesda, MD), normalized to GAPDH levels, and reported as relative intensity of the control.

Simultaneous EEG–ECG recordings

Mice of both sexes (ages 2–3 months) were anesthetized with avertin (0.02 ml/g, ip) and surgically implanted with bilateral silver wire electrodes (0.005-inch diameter) attached to a microminiature connector for recording in a tethered configuration. Electroencephalography (EEG) electrodes were inserted into the subdural space through cranial burr holes overlying left and right temporal cortex (for recording electrodes) and left and right frontal cortex (for reference and ground electrodes). For electrocardiography (ECG), two thoracic electrodes were tunneled subcutaneously on either side and sutured in place to

record cardiac activity. Mice were allowed to recover for 1 day before recording ~24 h of continuous EEG–ECG activity using a digital video EEG–ECG monitoring system (Data Sciences International; St Paul, MN). Signals were sampled at 1 kHz for EEG and 2 kHz for ECG.

The EEG–ECG recordings were analyzed offline using Ponemah software (Data Sciences International; St Paul, MN) to manually identify spontaneous seizures and cardiac events. The following digital filter settings were used for offline analysis unless otherwise stated: a 75-Hz low- and 0.3-Hz high-pass filter for EEG and a 3-Hz high-pass filter for ECG. Seizures were identified by visual inspection of the EEG and defined as high-amplitude (at least two times the baseline), rhythmic electrographic discharges lasting $\geq$ 5 s. Seizure frequency was calculated as the number of seizures per hour of recording, which was then expressed as seizures per 24 h. The seizure duration was defined as the time from the onset of electrographic seizure (usually a large high amplitude spike followed by sudden voltage depression) until the cessation of spiking. Seizure burden was calculated as the average time per h spent in seizure activity. SBSs were calculated as described previously by Roundtree *et al.* (64) by taking into account both seizure duration and behavioral seizure severity using the following equation: SBS = $\Sigma(\sigma_i\theta_i)$, where σ indicates the behavioral seizure severity score using the modified Racine scale, θ indicates the duration of each seizure, and i indicates each seizure. The modified Racine scale was the same as previously described in (16,64): stage 1, myoclonic jerk; stage 2, head nodding/stereotypy; stage 3, forelimb/hindlimb clonus, tail extension, a single rearing event; stage 4, continuous rearing and falling; and stage 5, severe tonic–clonic convulsions.

ECG waveforms were analyzed as previously described in (15). Briefly, all skipped heart beats were manually counted during the entire recording session. A skipped heart beat was defined as a prolongation of the RR interval equaling $\geq$ 1.5 times the previous RR interval. Skipped beats were usually associated with a non-conducted P-wave indicative of AV conduction block as previously described in (15). The average skipped heart beats per hour was defined as the total number of skipped beats divided by the total duration of recording hours.

EEG power spectrum analysis

EEG power spectral analysis was performed on 30-min samples of EEG recordings centered around ictal periods in *Kcna1*$^{-/-}$ and *Scn2a*$^{+/-}$*; Kcna1*$^{-/-}$ mice. The seizures in each mouse were categorized into three groups based on seizure duration, i.e. groups of short (<31 s), intermediate (31–60 s) and long (>60 s) seizure durations. For each mouse, the longest seizure per group was selected for study, such that one seizure per animal was analyzed in each group. Labchart 7 software (ADInstruments, Colorado Springs, CO) was used to create spectrograms and to determine spectral power density. In brief, each 30-min EEG sample was first passed through a 0.3–55 Hz band-pass digital filter and the Fast Fourier Method applied (FFT size 8192, Welch windowing with 93.75% windows overlap) to create spectrograms. We specifically focused on the pre- and post-ictal periods, which we defined as the 2-min time interval between 1 and 3 min prior to seizure onset and between 1 and 3 min after seizure termination, respectively. These 2-min windows of spectral data were analyzed using the data pad analysis module in Labchart to determine the relative spectral power of the five main EEG frequency bands (δ-band: 0.5–3 Hz; θ-band: 3.5–7 Hz; α-band: 8–12 Hz; β-band: 13–20 Hz; and γ-band: 21–50 Hz). The relative power of each band was expressed as the percentage of total spectral power between 0.5 and 50 Hz. Only EEG channels without noise and artifacts were considered and periods of EEG signals with significant artifacts were removed from the analysis.

Flurothyl-induced seizure susceptibility

Mice of both sexes (ages 2–3 months) were placed in an air-tight Plexiglass chamber (18.4 × 15.0 × 34.5 cm) and allowed to acclimate for 5 min. The liquid convulsant flurothyl (2,2,2-trifluoroethyl ether; Sigma-Aldrich, St Louis, MO) was then infused with a syringe pump at a rate of 20 µl/min onto Whatman filter paper suspended at the top of the chamber from which it vaporized. Observers blinded to genotype recorded the latencies (in seconds) from the first drip of flurothyl to the first myoclonic jerk and to generalized tonic–clonic seizure, which serve as measures of seizure threshold. Immediately following the onset of generalized seizures, mice were quickly removed from the chamber and placed in a cage with fresh air for observation and recovery. Each mouse was tested individually and received only one exposure to flurothyl. The testing chamber was cleaned and aerated before each trial.

HRV analysis

Ponemah software (Data Sciences International; St Paul, MN) was used to generate RR interval data for one 5-min ECG segment every 3 h during the 12-h light-phase period, for a total of four segments. ECG recordings were only selected for analysis during times when the animal was stationary and the data free of movement artifacts. HRV was measured in the time domain using the standard deviation of the RR intervals (SDNN) and the RMSSD, which were calculated using freely available Kubios HRV software (65). SDNN provides an index of total autonomic variability including both sympathetic (low frequency) and parasympathetic (high frequency) fluctuations, whereas RMSSD gives a measure of short-term variations in heart rate that reflect parasympathetic (vagal) influences (35).

Brain–heart association studies

The EEG record from each mouse was divided into 10-s sequential non-overlapping data segments. A second order IIR notch 60-Hz digital filter was applied to each EEG segment to filter out any interference in the recordings from power sources (line noise). Employing MATLAB's subroutine 'pca', principal component analysis was applied (66) to each pair of time-aligned 10-s segments from the two recording EEG electrodes to generate two linearly uncorrelated EEG signals (two principal components). The principal component (PC1(t)) signal exhibiting the highest energy, accounting for most of the variability in the analyzed EEGs within the 10-s period, was selected for further analysis. Fourth order Butterworth bandpass digital filters were applied to PC1(t) to further study its characteristics in the traditional EEG bands (δ = 0.5–3 Hz; θ = 3.5–7 Hz; α = 8–12 Hz; β = 13–20 Hz; and γ = 21–50 Hz). The Shannon entropy (ENT), a classical measure of a signal's complexity, was then estimated for every band-pass filtered 10-s segment of PC1(t) using a fixed number of bins in the construction of the related probability distribution (67). Thus, PC1(t)'s ENT_δ, ENT_θ, ENT_α, ENT_β and ENT_γ profiles over time per mouse were generated.

ECG was also divided into 10-s non-overlapping data segments, corresponding in time to the EEG data segments. Each ECG segment was then filtered by a digital fourth order Butterworth band pass (3–50 Hz) filter to remove the 60 Hz line noise and the wandering baseline in the ECG signal, and enable more accurate detection of the QRS complexes in the ECG. The QRS complexes were detected using the Pan-Tompkins algorithm (68) with detection thresholds adjusted for mouse ECG. The median length of the RR intervals (M_{RR}) was then estimated per segment over the duration of each recording. The median is more robust than the mean in the presence of outliers and noise in the data (69). Thus, the M_{RR} profile over time per mouse was generated. Additional measures of ECG dynamics and their temporal profiles were generated too. In total, for ECG measures of dynamics, the median, IQR and entropy of the RR intervals (M_{RR}, IQR_{RR}, ENT_{RR}) and of the R-peak values ($M_{R\text{-}peak}$, $IQR_{R\text{-}peak}$, $ENT_{R\text{-}peak}$) were employed.

Linear detrending of the brain's complexity and heart rate measures profiles was performed per mouse (MATLAB's subroutine 'nandetrend') to remove any persistent long-term (hours) linear trends in the data. After detrending, the resulting values of the EEG and ECG measures per 10-s segment were binarized with respect to their medians per mouse (assigning a value of 1 if a value was larger than the global median, and 0 otherwise). The degree of association between the EEG and ECG binarized measures was then evaluated over the whole record per mouse using the φ coefficient (70). High values of φ coefficients denote high association levels. φ coefficients are more robust than correlation or Pearson's coefficients in quantifying the relationship between signals since they do not deal with the raw data themselves but with the relative (binary) rankings of their values with respect to their own median values. Therefore, use of φ coefficients avoids an excessive impact of possible outlier values on the quantification of the EEG–ECG relationship. The trade-off of this strict 'filtering' process is that the association rather than the correlation between signals is thus quantified.

Statistical analysis

All data are expressed as means ± S.E.M. unless otherwise stated. Prism 6 for Windows (GraphPad Software Inc, La Jolla, CA) was used for statistical analysis. Survival curves were evaluated using the Kaplan-Meier log rank (Mantel-Cox) test. For comparisons involving only two groups, unpaired two-tailed Student's *t* tests were employed, except for comparisons of pre- and post-ictal EEG spectral profiles, which were evaluated using paired two-tailed Student's *t* tests. For comparisons involving three or more groups, one-way ANOVA was performed with Tukey's multiple comparison *post hoc* tests. Statistically significant differences between the φ coefficients across genotypes were assessed by Welch's ANOVA, and simple linear regression was used to identify the relationship between the φ coefficients and survival rate. In these two cases the *P*-values were adjusted for multiple comparisons (multiple pairs of EEG and ECG measures) by the BH step-up FDR control procedure (71). *P*-values < 0.05 were considered to denote statistical significance.

Supplementary Material

Supplementary material is available at *HMG* online.

Conflict of Interest statement. E.G., L.I. and I.V. have a United States provisional patent (No. 62/027,521) for the interaction dynamics technique described herein.

Funding

This work was supported by the US National Institutes of Health (grants R21NS089397 and R00HL107641 to E.G.), Citizens United for Research in Epilepsy (grant 354389 to E.G. and L.I.), and the US National Science Foundation (grant EPSCoR RII Track-2 FEC 1632891 to L.I.).

References

1. Goldman, A.M., Behr, E.R., Semsarian, C., Bagnall, R.D., Sisodiya, S. and Cooper, P.N. (2016) Sudden unexpected death in epilepsy genetics: Molecular diagnostics and prevention. *Epilepsia*, **57(Suppl 1)**, 17–25.
2. Glasscock, E. (2014) Genomic biomarkers of SUDEP in brain and heart. *Epilepsy Behav.*, **38**, 172–179.
3. Nashef, L., So, E.L., Ryvlin, P. and Tomson, T. (2012) Unifying the definitions of sudden unexpected death in epilepsy. *Epilepsia*, **53**, 227–233.
4. Ryvlin, P., Nashef, L., Lhatoo, S.D., Bateman, L.M., Bird, J., Bleasel, A., Boon, P., Crespel, A., Dworetzky, B.A., Høgenhaven, H. *et al.* (2013) Incidence and mechanisms of cardiorespiratory arrests in epilepsy monitoring units (MORTEMUS): a retrospective study. *Lancet Neurol.*, **12**, 966–977.
5. Thurman, D.J., Hesdorffer, D.C. and French, J.A. (2014) Sudden unexpected death in epilepsy: assessing the public health burden. *Epilepsia*, **55**, 1479–1485.
6. Noebels, J. (2015) Pathway-driven discovery of epilepsy genes. *Nat. Neurosci.*, **18**, 344–350.
7. Klassen, T., Davis, C., Goldman, A., Burgess, D., Chen, T., Wheeler, D., McPherson, J., Bourquin, T., Lewis, L., Villasana, D. *et al.* (2011) Exome sequencing of ion channel genes reveals complex profiles confounding personal risk assessment in epilepsy. *Cell*, **145**, 1036–1048.
8. Leu, C., Balestrini, S., Maher, B., Hernández-Hernández, L., Gormley, P., Hämäläinen, E., Heggeli, K., Schoeler, N., Novy, J., Willis, J. *et al.* (2015) Genome-wide Polygenic Burden of Rare Deleterious Variants in Sudden Unexpected Death in Epilepsy. *EBioMedicine*, **2**, 1063–1070.
9. Bagnall, R.D., Crompton, D.E., Petrovski, S., Lam, L., Cutmore, C., Garry, S.I., Sadleir, L.G., Dibbens, L.M., Cairns, A., Kivity, S. *et al.* (2016) Exome-based analysis of cardiac arrhythmia, respiratory control, and epilepsy genes in sudden unexpected death in epilepsy. *Ann. Neurol.*, **79**, 522–534.
10. Tempel, B.L., Jan, Y.N. and Jan, L.Y. (1988) Cloning of a probable potassium channel gene from mouse brain. *Nature*, **332**, 837–839.
11. Kamb, A., Iverson, L.E. and Tanouye, M.A. (1987) Molecular characterization of Shaker, a Drosophila gene that encodes a potassium channel. *Cell*, **50**, 405–413.
12. Jan, L.Y. and Jan, Y.N. (2012) Voltage-gated potassium channels and the diversity of electrical signalling. *J. Physiol.*, **590**, 2591–2599.
13. Smart, S.L., Lopantsev, V., Zhang, C.L., Robbins, C.A., Wang, H., Chiu, S.Y., Schwartzkroin, P.A., Messing, A. and Tempel, B.L. (1998) Deletion of the K(V)1.1 potassium channel causes epilepsy in mice. *Neuron*, **20**, 809–819.
14. Moore, B.M., Jerry Jou, C., Tatalovic, M., Kaufman, E.S., Kline, D.D. and Kunze, D.L. (2014) The Kv1.1 null mouse, a model of sudden unexpected death in epilepsy (SUDEP). *Epilepsia*, **55**, 1808–1816.
15. Glasscock, E., Yoo, J.W., Chen, T.T., Klassen, T.L. and Noebels, J.L. (2010) Kv1.1 potassium channel deficiency

reveals brain-driven cardiac dysfunction as a candidate mechanism for sudden unexplained death in epilepsy. *J. Neurosci.*, **30**, 5167–5175.
16. Simeone, K.A., Matthews, S.A., Rho, J.M. and Simeone, T.A. (2016) Ketogenic diet treatment increases longevity in Kcna1-null mice, a model of sudden unexpected death in epilepsy. *Epilepsia*, **57**, e178–e182.
17. Fenoglio-Simeone, K.A., Wilke, J.C., Milligan, H.L., Allen, C.N., Rho, J.M. and Maganti, R.K. (2009) Ketogenic diet treatment abolishes seizure periodicity and improves diurnal rhythmicity in epileptic Kcna1-null mice. *Epilepsia*, **50**, 2027–2034.
18. Browne, D.L., Gancher, S.T., Nutt, J.G., Brunt, E.R., Smith, E.A., Kramer, P. and Litt, M. (1994) Episodic ataxia/myokymia syndrome is associated with point mutations in the human potassium channel gene, KCNA1. *Nat. Genet.*, **8**, 136–140.
19. Zuberi, S.M., Eunson, L.H., Spauschus, A., De Silva, R., Tolmie, J., Wood, N.W., McWilliam, R.C., Stephenson, J.B., Stephenson, J.P., Kullmann, D.M. *et al.* (1999) A novel mutation in the human voltage-gated potassium channel gene (Kv1.1) associates with episodic ataxia type 1 and sometimes with partial epilepsy. *Brain*, **122 (Pt 5)**, 817–825.
20. Kinali, M., Jungbluth, H., Eunson, L.H., Sewry, C.A., Manzur, A.Y., Mercuri, E., Hanna, M.G. and Muntoni, F. (2004) Expanding the phenotype of potassium channelopathy: severe neuromyotonia and skeletal deformities without prominent Episodic Ataxia. *Neuromuscul. Disord.*, **14**, 689–693.
21. Graves, T.D., Rajakulendran, S., Zuberi, S.M., Morris, H.R., Schorge, S., Hanna, M.G. and Kullmann, D.M. (2010) Nongenetic factors influence severity of episodic ataxia type 1 in monozygotic twins. *Neurology*, **75**, 367–372.
22. Demos, M.K., Macri, V., Farrell, K., Nelson, T.N., Chapman, K., Accili, E. and Armstrong, L. (2009) A novel KCNA1 mutation associated with global delay and persistent cerebellar dysfunction. *Mov. Disord.*, **24**, 778–782.
23. Liguori, R., Avoni, P., Baruzzi, A., Di Stasi, V. and Montagna, P. (2001) Familial continuous motor unit activity and epilepsy. *Muscle Nerve*, **24**, 630–633.
24. D'Adamo, M.C., Hasan, S., Guglielmi, L., Servettini, I., Cenciarini, M., Catacuzzeno, L. and Franciolini, F. (2015) New insights into the pathogenesis and therapeutics of episodic ataxia type 1. *Front. Cell. Neurosci.*, **9**, 317.
25. Klassen, T.L., Bomben, V.C., Patel, A., Drabek, J., Chen, T.T., Gu, W., Zhang, F., Chapman, K., Lupski, J.R., Noebels, J.L. *et al.* (2014) High-resolution molecular genomic autopsy reveals complex sudden unexpected death in epilepsy risk profile. *Epilepsia*, **55**, e6–12.
26. Rodríguez-Calvo, M.S., Brion, M., Allegue, C., Concheiro, L. and Carracedo, A. (2008) Molecular genetics of sudden cardiac death. *Forensic Sci. Int.*, **182**, 1–12.
27. Glasscock, E., Qian, J., Yoo, J.W. and Noebels, J.L. (2007) Masking epilepsy by combining two epilepsy genes. *Nat. Neurosci.*, **10**, 1554–1558.
28. Holth, J.K., Bomben, V.C., Reed, J.G., Inoue, T., Younkin, L., Younkin, S.G., Pautler, R.G., Botas, J. and Noebels, J.L. (2013) Tau loss attenuates neuronal network hyperexcitability in mouse and Drosophila genetic models of epilepsy. *J. Neurosci.*, **33**, 1651–1659.
29. Boiko, T., Rasband, M.N., Levinson, S.R., Caldwell, J.H., Mandel, G., Trimmer, J.S. and Matthews, G. (2001) Compact myelin dictates the differential targeting of two sodium channel isoforms in the same axon. *Neuron*, **30**, 91–104.
30. Boiko, T., Van Wart, A., Caldwell, J.H., Levinson, S.R., Trimmer, J.S. and Matthews, G. (2003) Functional specialization of the axon initial segment by isoform-specific sodium channel targeting. *J. Neurosci.*, **23**, 2306–2313.
31. Planells-Cases, R., Caprini, M., Zhang, J., Rockenstein, E.M., Rivera, R.R., Murre, C., Masliah, E. and Montal, M. (2000) Neuronal death and perinatal lethality in voltage-gated sodium channel alpha(II)-deficient mice. *Biophys. J.*, **78**, 2878–2891.
32. Yang, L., Worrell, G.A., Nelson, C., Brinkmann, B. and He, B. (2012) Spectral and spatial shifts of post-ictal slow waves in temporal lobe seizures. *Brain*, **135**, 3134–3143.
33. Prichard, J.W., Gallagher, B.B. and Glaser, G.H. (1969) Experimental seizure-threshold testing with fluorthyl. *J. Pharmacol. Exp. Ther.*, **166**, 170–178.
34. Rho, J.M., Szot, P., Tempel, B.L. and Schwartzkroin, P.A. (1999) Developmental seizure susceptibility of kv1.1 potassium channel knockout mice. *Dev. Neurosci.*, **21**, 320–327.
35. Stables, C.L., Auerbach, D.S., Whitesall, S.E., D'Alecy, L.G. and Feldman, E.L. (2016) Differential impact of type-1 and type-2 diabetes on control of heart rate in mice. *Auton. Neurosci. Basic Clin.*, **194**, 17–25.
36. Kearney, J.A. (2011) Genetic modifiers of neurological disease. *Curr. Opin. Genet. Dev.*, **21**, 349–353.
37. Liao, Y., Deprez, L., Maljevic, S., Pitsch, J., Claes, L., Hristova, D., Jordanova, A., Ala-Mello, S., Bellan-Koch, A., Blazevic, D. *et al.* (2010) Molecular correlates of age-dependent seizures in an inherited neonatal-infantile epilepsy. *Brain*, **133**, 1403–1414.
38. Robbins, C.A. and Tempel, B.L. (2012) Kv1.1 and Kv1.2: similar channels, different seizure models. *Epilepsia*, **53 Suppl 1**, 134–141.
39. Aiba, I. and Noebels, J.L. (2015) Spreading depolarization in the brainstem mediates sudden cardiorespiratory arrest in mouse SUDEP models. *Sci. Transl. Med.*, **7**, 282ra46.
40. Fletcher, C.F., Lutz, C.M., O'Sullivan, T.N., Shaughnessy, J.D., Hawkes, R., Frankel, W.N., Copeland, N.G. and Jenkins, N.A. (1996) Absence epilepsy in tottering mutant mice is associated with calcium channel defects. *Cell*, **87**, 607–617.
41. Qian, J. and Noebels, J.L. (2000) Presynaptic Ca(2+) influx at a mouse central synapse with Ca(2+) channel subunit mutations. *J. Neurosci.*, **20**, 163–170.
42. Morris, M., Maeda, S., Vossel, K. and Mucke, L. (2011) The many faces of tau. *Neuron*, **70**, 410–426.
43. Misra, S.N., Kahlig, K.M. and George, A.L. (2008) Impaired NaV1.2 function and reduced cell surface expression in benign familial neonatal-infantile seizures. *Epilepsia*, **49**, 1535–1545.
44. Kamiya, K., Kaneda, M., Sugawara, T., Mazaki, E., Okamura, N., Montal, M., Makita, N., Tanaka, M., Fukushima, K., Fujiwara, T. *et al.* (2004) A nonsense mutation of the sodium channel gene SCN2A in a patient with intractable epilepsy and mental decline. *J. Neurosci. Off. J. Soc. Neurosci.*, **24**, 2690–2698.
45. Oliva, M., Berkovic, S.F. and Petrou, S. (2012) Sodium channels and the neurobiology of epilepsy. *Epilepsia*, **53**, 1849–1859.
46. de Ligt, J., Willemsen, M.H., van Bon, B.W.M., Kleefstra, T., Yntema, H.G., Kroes, T., Vulto-van Silfhout, A.T., Koolen, D.A., de Vries, P., Gilissen, C. *et al.* (2012) Diagnostic exome sequencing in persons with severe intellectual disability. *N. Engl. J. Med.*, **367**, 1921–1929.
47. Carvill, G.L., Heavin, S.B., Yendle, S.C., McMahon, J.M., O'Roak, B.J., Cook, J., Khan, A., Dorschner, M.O., Weaver, M., Calvert, S. *et al.* (2013) Targeted resequencing in epileptic encephalopathies identifies de novo mutations in CHD2 and SYNGAP1. *Nat. Genet.*, **45**, 825–830.

48. Howell, K.B., McMahon, J.M., Carvill, G.L., Tambunan, D., Mackay, M.T., Rodriguez-Casero, V., Webster, R., Clark, D., Freeman, J.L., Calvert, S. *et al.* (2015) SCN2A encephalopathy: A major cause of epilepsy of infancy with migrating focal seizures. *Neurology*, **85**, 958–966.
49. Rauch, A., Wieczorek, D., Graf, E., Wieland, T., Endele, S., Schwarzmayr, T., Albrecht, B., Bartholdi, D., Beygo, J., Di Donato, N. *et al.* (2012) Range of genetic mutations associated with severe non-syndromic sporadic intellectual disability: an exome sequencing study. *Lancet Lond. Engl.*, **380**, 1674–1682.
50. Sanders, S.J., Murtha, M.T., Gupta, A.R., Murdoch, J.D., Raubeson, M.J., Willsey, A.J., Ercan-Sencicek, A.G., DiLullo, N.M., Parikshak, N.N., Stein, J.L. *et al.* (2012) De novo mutations revealed by whole-exome sequencing are strongly associated with autism. *Nature*, **485**, 237–241.
51. Westenbroek, R.E., Bischoff, S., Fu, Y., Maier, S.K.G., Catterall, W.A. and Scheuer, T. (2013) Localization of sodium channel subtypes in mouse ventricular myocytes using quantitative immunocytochemistry. *J. Mol. Cell. Cardiol.*, **64**, 69–78.
52. Abdelsayed, M. and Sokolov, S. (2013) Voltage-gated sodium channels: pharmaceutical targets via anticonvulsants to treat epileptic syndromes. *Channels*, **7**, 146–152.
53. Catterall, W.A. (2014) Sodium channels, inherited epilepsy, and antiepileptic drugs. *Annu. Rev. Pharmacol. Toxicol.*, **54**, 317–338.
54. Lavebratt, C., Trifunovski, A., Persson, A.-S., Wang, F.-H., Klason, T., Ohman, I., Josephsson, A., Olson, L., Spenger, C. and Schalling, M. (2006) Carbamazepine protects against megencephaly and abnormal expression of BDNF and Nogo signaling components in the mceph/mceph mouse. *Neurobiol. Dis.*, **24**, 374–383.
55. Stefani, A., Spadoni, F., Siniscalchi, A. and Bernardi, G. (1996) Lamotrigine inhibits Ca2+ currents in cortical neurons: functional implications. *Eur. J. Pharmacol.*, **307**, 113–116.
56. Zona, C., Tancredi, V., Longone, P., D'Arcangelo, G., D'Antuono, M., Manfredi, M. and Avoli, M. (2002) Neocortical potassium currents are enhanced by the antiepileptic drug lamotrigine. *Epilepsia*, **43**, 685–690.
57. Liao, W.-P., Shi, Y.-W., Long, Y.-S., Zeng, Y., Li, T., Yu, M.-J., Su, T., Deng, P., Lei, Z.-G., Xu, S.-J. *et al.* (2010) Partial epilepsy with antecedent febrile seizures and seizure aggravation by antiepileptic drugs: associated with loss of function of Na(v) 1.1. *Epilepsia*, **51**, 1669–1678.
58. Guerrini, R., Dravet, C., Genton, P., Belmonte, A., Kaminska, A. and Dulac, O. (1998) Lamotrigine and seizure aggravation in severe myoclonic epilepsy. *Epilepsia*, **39**, 508–512.
59. Jouny, C.C., Franaszczuk, P.J. and Bergey, G.K. (2011) Improving early seizure detection. *Epilepsy Behav.*, **22(Suppl 1)**, S44–S48.
60. Iasemidis, L.D. (2011) Seizure prediction and its applications. *Neurosurg. Clin. N. Am.*, **22**, 489–506, vi.
61. Sabesan, S., Good, L.B., Tsakalis, K.S., Spanias, A., Treiman, D.M. and Iasemidis, L.D. (2009) Information flow and application to epileptogenic focus localization from intracranial EEG. *IEEE Trans. Neural Syst. Rehabil. Eng.*, **17**, 244–253.
62. Valenza, G., Toschi, N. and Barbieri, R. (2016) Uncovering brain-heart information through advanced signal and image processing. *Philos. Trans. A Math. Phys. Eng. Sci.*, **374**, 1–6.
63. Gautier, N.M. and Glasscock, E. (2015) Spontaneous seizures in Kcna1-null mice lacking voltage-gated Kv1.1 channels activate Fos expression in select limbic circuits. *J. Neurochem.*, **135**, 157-164.
64. Roundtree, H.M., Simeone, T.A., Johnson, C., Matthews, S.A., Samson, K.K. and Simeone, K.A. (2016) Orexin receptor antagonism improves sleep and reduces seizures in Kcna1-null mice. *Sleep*, **39**, 357–368.
65. Tarvainen, M.P., Niskanen, J.-P., Lipponen, J.A., Ranta-Aho, P.O. and Karjalainen, P.A. (2014) Kubios HRV–heart rate variability analysis software. *Comput. Methods Programs Biomed.*, **113**, 210–220.
66. Jolliffe, I.T. (2002) *Principal Component Analysis*, 2nd edn. Springer-Verlag, New York.
67. Pezard, L., Martinerie, J., Müller-Gerking, J., Varela, F.J. and Renault, B. (1996) Entropy quantification of human brain spatio-temporal dynamics. *Phys. Nonlinear Phenom.*, **96**, 344–354.
68. Pan, J. and Tompkins, W.J. (1985) A Real-Time QRS Detection Algorithm. *IEEE Trans. Biomed. Eng.*, **BME-32**, 230–236.
69. Devore, J.L. (2012) *Probability and Statistics for Engineering and the Sciences*, 8th edn. Cengage Learning, Boston, MA.
70. Everitt, B. and Skrondal, A. (2010) *The Cambridge Dictionary of Statistics*, 4th edn. Cambridge University Press, Cambridge.
71. Benjamini, Y. and Hochberg, Y. (1995) Controlling the false discovery rate: a practical and powerful approach to multiple testing. *J. R. Stat. Soc. B*, **57**, 289–300.